Implementation of PI Control for Angular Speed Regulation in Magnetic Levitation Systems

1st Missael Becerra-Aguilera
UPIIZ-IPN
Zacatecas, México
0009-0009-1488-0997

2nd Juan Landeros-Saucedo
UPIIZ-IPN
Zacatecas, México
0009-0007-0026-9172

3rd Umanel Hernández-González
UPIIZ-IPN
Zacatecas, México
0000-0002-4109-1776

4th Sergio Domínguez-Sánchez
UPIIZ-IPN
Zacatecas, México
0000-0002-9891-7858

5th Flabio Mirelez-Delgado
UPIIZ-IPN
Zacatecas, México
0000-0003-3547-9739

***Abstract*—This paper presents the design, implementation, and control of a magnetic levitation and rotation system oriented to low-maintenance rotational applications. The prototype consists of a magnetic levitator capable of supporting up to 700 g and a circular array of 12 electromagnets (to be referred to hereinafter as electromagnetic actuators), which, through an on/off controlled sequence, generates angular motion of a levitated platform. The platform is 304.8 mm in diameter and incorporates a neodymium magnet in the center for levitation and four magnets at its ends, which are sequentially activated by the electromagnetic actuators to induce rotation. An adaptive PID control system executed in an ESP32 WROOM-32 microcontroller was implemented, whose feedback is obtained through a Hall effect sensor (LM393 3144). The characterization of the system was performed by identifying a transfer function based on the inverse curve of the deceleration response, which allowed adjusting the gains of the PID controller to achieve a response with an overshoot of 10% and a settling time of 120 s. Experimental tests at 33, 45, and 78 revolutions per minute (RPM) showed that, although the system operates robustly at low speeds, at higher speeds, longer settling times and response variability are evident. The results obtained confirm the feasibility of the proposed approach and open lines of improvement in control optimization for industrial and academic applications. The main contributions of this work are summarized as the development of a functional prototype of a magnetic levitation and rotation system inspired by turntable platforms, integrating permanent magnets and a 12 electromagnet array to enable contactless angular motion and the implementation of an adaptive PI control system using a Hall effect sensor for closed-loop speed regulation for said system.**

***Index Terms*—Magnetic levitation; PI control; Levitated platform; Electromagnets; Magnetically induced angular acceleration.**

I. Introduction

Magnetic levitation (Maglev) has been studied in various fields in order to facilitate its application in systems ranging from industrial transportation [1] to the analysis of microstructures such as cells or proteins [2]. Thus, it is possible to generalize that the use of Maglev systems is considered for applications where significantly reducing friction and mechanical wear is a benefit [3], [4].

Following this idea, comes to mind the development of levitation systems that combine permanent magnets (PMs, which after being magnetized by a high magnetic field, maintain their high magnetization even with temperature changes or with the presence of external magnetic fields [5]) with electromagnets to achieve not only contactless suspension, but also precise control of parameters such as levitation height or stability. There are examples of vehicle applications on trains [6] as well as general linear actuators [7] that test the integration of control and optimization techniques [8] to fine-tune system behavior, even in the face of its natural complexity.

This paper takes Maglev technology and the idea of employing it for the purpose of generating motion, and addresses the design and control of an approximately 30 cm platform levitation and rotation system to demonstrate the feasibility of magnetic levitation for low-maintenance rotational applications with a focus on future applications in rotational systems, as well as for academic demonstration.

Conceptually, the idea of generating angular motion using magnetic forces is not new, as the lack of any mechanical elements involved ideally allows for the reduction of vibration and friction. For example, "Polarity Free Magnetic Repulsion and Magnetic Bound State" [9], work by Hamdi Ucar offers a magnetic rotation and levitation system, in which levitation is achieved by a magnet rotating at an approximate 200 Hz rotational frequency. This causes levitation of another magnet in its vicinity, however, the rotational speed cannot be easily controlled, especially if one expects to slow down the speed without compromising levitation. The present paper details a magnetic levitator and rotator design, a system composed of two independent elements: (1) a magnetic levitator with a weight capacity of up to 700 g, responsible for maintaining the suspension of the elements to be levitated, and (2) a circular array of 12 electromagnetic actuators that generate angular motion through a controlled on/off sequence.

The platform (to be referred to hereinafter as the levitated platform) consists of a 304.8 mm (12 in.) circular disk with a neodymium magnet in the center, and four neodymium

magnets at the ends of the levitated platform. The central magnet serves to levitate, while the magnets on the edges are driven by the electromagnetic actuators by turning themselves off and on sequentially in a clockwise direction, generating angular motion. An adaptive PID control system is used, whose feedback is obtained by means of a hall effect sensor LM393 3144 that serves as a tachometer of the levitated platform, allowing to know the number of RPM to be known through a code executed in the ESP32 WROOM-32 microcontroller.

The rest of the paper is organized as follows: The elements involved in magnetic levitation and rotation, as well as the control methodology involved, are presented in Section 2. Experimental results are illustrated in Section 3. Finally, section 4 concludes the paper and opens space for discussion.

II. Material and Method

A. Levitation

1) Magnetic Levitator: The experimental prototype incorporates a commercial magnetic levitation module. Its features include the ability to suspend a load of up to 700 g, with a levitation height of approximately 10.8-20.5 cm above the base. The device has four 5 V, 0.2 A solenoidal lifting electromagnets at its center, which, supported by a surrounding ferrite magnet, employ electromagnetic feedback to maintain the levitation of a 50.0 mm diameter neodymium disc. The magnetic levitation module employed is visible in Fig. 1.

2) Levitated platform: The levitated platform is a circular disk of 304.8 mm, made of polylactic acid (PLA) with a central slot of 50.0 mm diameter in which a neodymium disk is inserted to generate levitation (to be referred to hereinafter as the central neodymium disk). Similarly, the outer perimeter of the levitated platform incorporates four circular neodymium magnets equidistant from each other, whose magnetic fields are used for rotation control. The fabrication of the levitated platform was made in consideration of the levitated weight limit of the magnetic levitator. When approaching this limit, the levitation height decreases, which increases the risk of a magnetic imbalance that interrupts the levitation state. Adding up all the elements of the levitated platform, the total weight is 476 g, in which the central neodymium disk weighs 160 g, the 4 outer neodymium magnets total 140 g, and the levitated platform structure weighs 176 g.

Fig. 1: Magnetic levitator module and its dimensions.

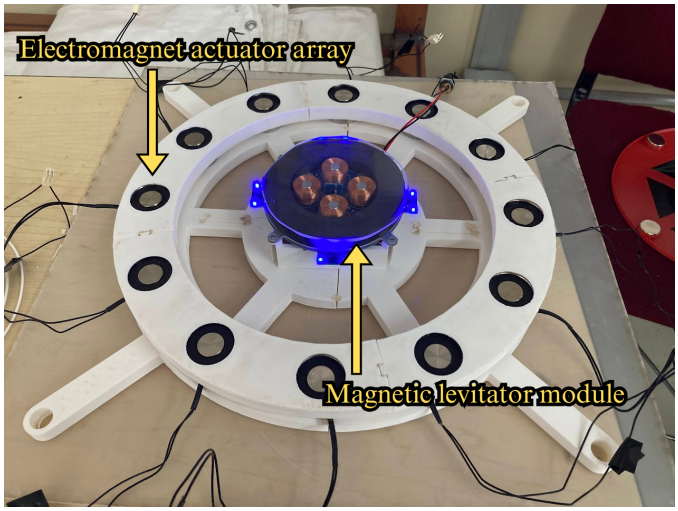

Fig. 2: Circular electromagnet actuator array and magnetic levitator module.

B. Rotation

For the generation of a controlled angular motion, an array of 12 solenoid lifting electromagnets with 12 V, 0.5 A electrical characteristics, arranged in a circular equidistant array around the magnetic levitation module, was employed. The idea behind this topology, visible in Fig. 2, is to control the on/off sequence of these electromagnetic actuators in order to generate an acceleration by interacting with the magnetic fields of 4 neodymium magnets arranged on the levitated platform.

For this purpose, a control sequence is implemented to keep 8 electromagnetic actuators on simultaneously, repelling the magnets on the platform at all times and leaving 4 electromagnetic actuators off, which causes the magnets to move until they are over the off electromagnetic actuators (see Fig. 3). By changing the sequence, the actuators are turned on and off sequentially, so that the off electromagnet is always next to the magnet on the platform in a clockwise direction, thus generating the rotational motion whose velocity is decided by the control interface that allows the selection of 3 different speeds, 33, 45 and 78 RPM.

The position of the levitated platform is fed back by one Hall effect sensors that detect the passage of the magnets on the platform by being positioned parallel to the levitated platform, generating 4 pulses per revolution, which provides the necessary feedback to adjust the speed of the platform. For the control stage, it was decided to use a Proportional-Integral-

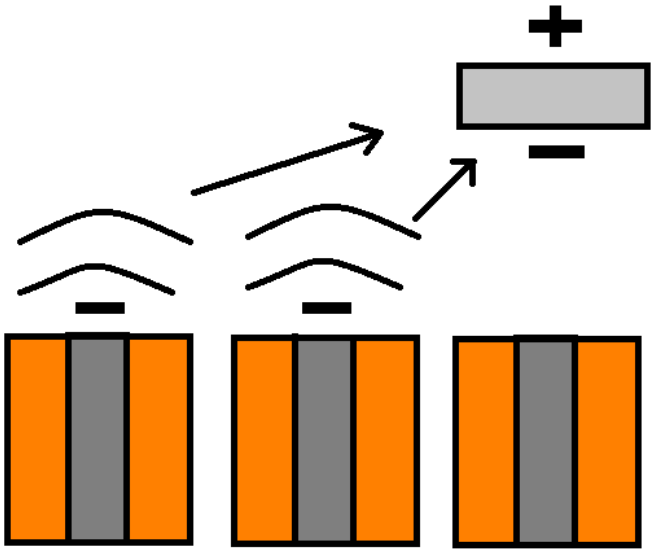

Fig. 3: Control sequence diagram.

Derivative (PID) control since the system has no physical connection and any external force can cause variations in the behavior. In addition, the platform's inertia difficult to achieve a fast deceleration, since the magnetic fields cannot generate excessive forces without causing vibrations that could destabilize the levitation.

Since the system is not capable of accelerating on its own without active control, it was not possible to obtain a direct startup curve. Therefore, we opted to characterize the system's behavior using the inverse curve. This procedure consisted of manually accelerating the levitated platform up to approximately 60 RPM and recording its natural deceleration. Fig. 4 shows the deceleration curve, obtained by analyzing the Hall effect sensor data collected from the microcontroller.

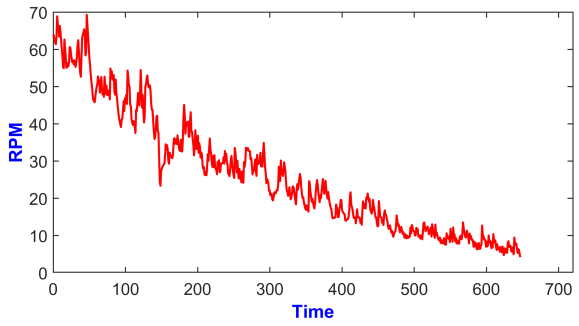

Fig. 4: Experimental deceleration curve of the levitated platform, used for inverse response characterization to estimate the system's transfer function.

Assuming that the system has the same behavior on acceleration stage, Figure 5 shows how the system would begin to spin and Figure 6 depicts how the data can fit into a first order time response, but for analysis purpose it will be model as a second order system.

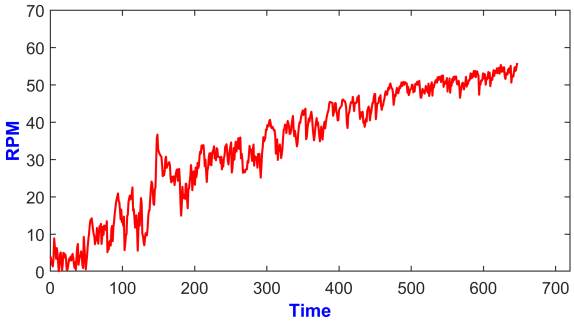

Fig. 5: System's acceleration behavior.

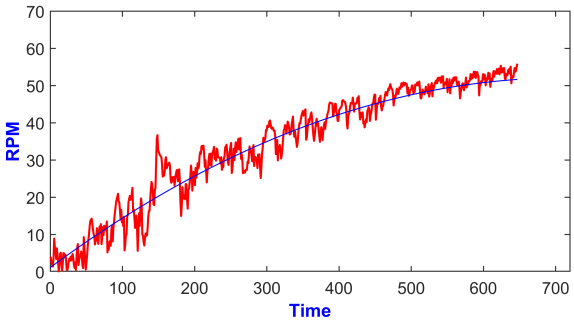

Fig. 6: System approximation.

C. Control

Based on the graph of the system's deceleration behavior, a transfer function was estimated that approximately reflected this response, despite the noise present due to time shifts between sampling and data acquisition. The transfer function was obtained using MATLAB software to process and filter the data acquired from the Hall effect sensor, thereby producing a graph that represents the system without excessive noise, as shown in Fig. 7.

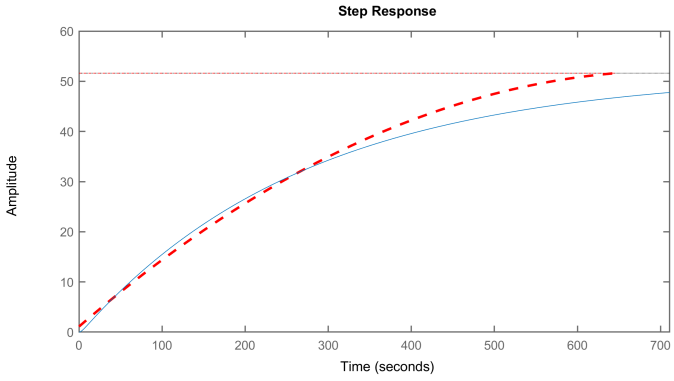

Fig. 7: Comparison between estimated transfer function and experimental system behavior.

To obtain the system's transfer function, the 63.2% point on the graph was calculated along with its corresponding time in the simplified inverse response curve of the system, which was determined to be 272 s, yielding a pole at $s_2 = -0.0037$. Additionally, the settling time was determined to be 51 RPM;

using these values, the transfer function was approximated as a second-order system. The second pole was calculated with (1).

$$s_1 = \omega_n(\zeta + \sqrt{\zeta^2 - 1}) = 0.3591 \tag{1}$$

This simplification allowed for the integration of a PID controller, giving the following second-order transfer function model:

$$\frac{0.06795}{s^2 + 0.3628s + 0.001316} \tag{2}$$

With the obtained transfer function, the desired time response was designed targeting an overshoot of 10% and a settling time of 210 s. Since the system does not have direct contact between the levitated platform and the elements that induce angular motion, but rather they are separated by approximately 60.0 mm, there is insufficient electromagnetic power to generate an immediate angular impulse to reach the desired speed. As observed in Fig. 4 and 7, the speed change requires a considerable amount of time. Consequently, a duration of approximately 3 minutes and 30 seconds was deemed adequate for the magnetic fields to bring the platform to the set speed.

To calculate the control law, the damping factor and the desired natural frequency of the system were first determined using (3) and (4), respectively.

$$\zeta = \frac{1}{\sqrt{\left(\frac{\pi}{-ln(Mp)}\right)^2 + 1}} = \frac{1}{\sqrt{\left(\frac{\pi}{-ln(0.1)}\right)^2 + 1}} = 0.5912 \tag{3}$$

$$\omega_n = \frac{4}{t_s\zeta} = \frac{4}{(210)(0.5912)} = 0.0322 \tag{4}$$

Thus, the desired real and imaginary parts for the pole locations were determined using (5) and (6), respectively.

$$\sigma = \zeta\omega_n = (0.5912)(0.0322) = 0.019 \tag{5}$$

$$\omega_d = \omega_n\sqrt{1 - \zeta^2} = 0.0322\sqrt{1 - 0.5912^2} = 0.026 \tag{6}$$

Therefore, the desired pole locations (Fig. 8) should be at:

$$-0.0190 \pm 0.0260i \tag{7}$$

As can be seen in Figures 4 and 7, the system's time response is slow, thus, there is no need to calculate a PD controller or a derivative action. Instead, calculations will be over the PI controller.

To determine the controller's zero location that would place the system poles at the desired positions, Equation (8) was used to find the zero's angle with respect to the system poles and the desired location, considering the angles in Figure 9:

$$\theta_{z_c} - \theta_{s=-0.0037} - \theta_{s=-0.3591} - \theta_{s=0} = \pm(2k-1)180^\circ \tag{8}$$

Substituting the known values in (8),

$$\theta_{z_c} - 120.62^\circ - 4.36^\circ - 126.33^\circ = \pm(2k-1)180^\circ \tag{9}$$

We obtain with (9), the zero angle given by:

$$\theta_{z_c} = 71.23^\circ \tag{10}$$

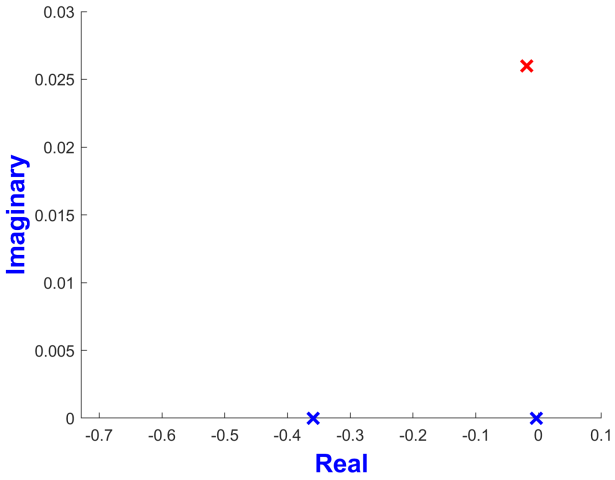

Fig. 8: Desired dominant poles (red) and system poles (blue).

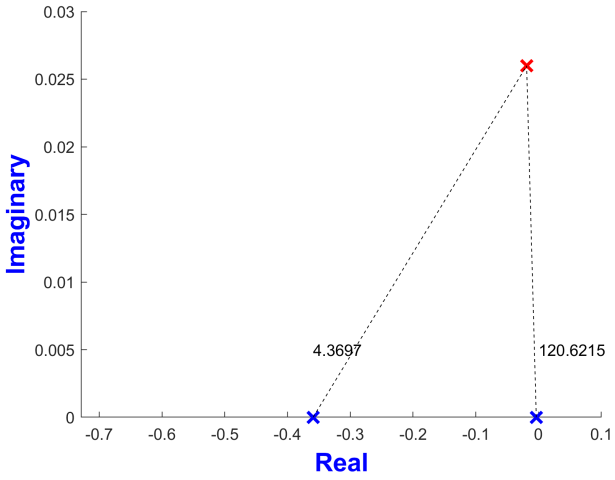

Fig. 9: Angles among desired dominant poles and system poles.

Thus, the zero location of the controller was calculated with (11) to accomplish the angle condition:

$$\begin{aligned} d &= \omega_d / \tan(\theta_{z_c})) = 0.0088 \\ z_c &= -(\sigma + d) = -0.0279 \end{aligned} \tag{11}$$

Next, to calculate the control gain (K) of the PI controller, (12) was used considering the system, the PI pole at the origin, and the PI's zero to satisfy the magnitude condition:

$$\left| K\frac{(s + 0.0279)}{s(s + 0.3591)(s + 0.0037)} \right| = 1 \tag{12}$$

Substituting s with the desired pole location and solving, the controller gain was found to be (13):

$$K = 2.3424e - 04 \tag{13}$$

Based on this, the control gains were calculated, yielding the integration time, the proportional gain, and the integration

gain with (14), (15), and (16) respectively.

$$T_i = 1/z_c = 35.8688 \tag{14}$$
$$K_p = K = 2.3424e-04 \tag{15}$$
$$K_i = K_p/t_i = 6.5306e-06 \tag{16}$$

Resulting in a control system given by the following transfer function with the poles of the system and one pole and one zero of control PI, obtaining the following third-order function (17):

$$\frac{0.012s + 0.00034}{s^3 + 0.36s^2 + 0.0013s} \tag{17}$$

The root locus for the control system is shown in Figure 10 and its temporal response in Figure 11. As can be seen, the root locus passes through the desired dominant poles, and the time response achieves the desired value of 33 RPM.

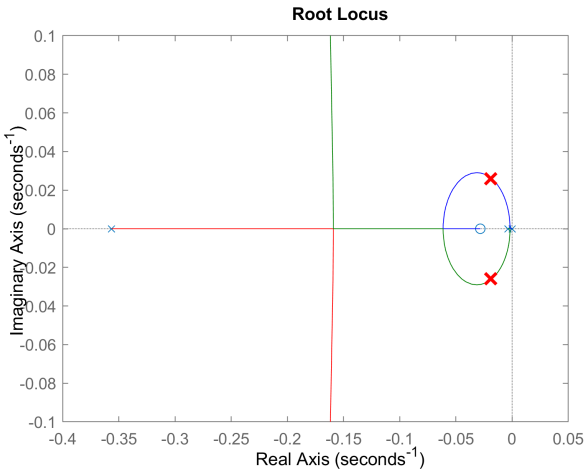

Fig. 10: Control system root locus.

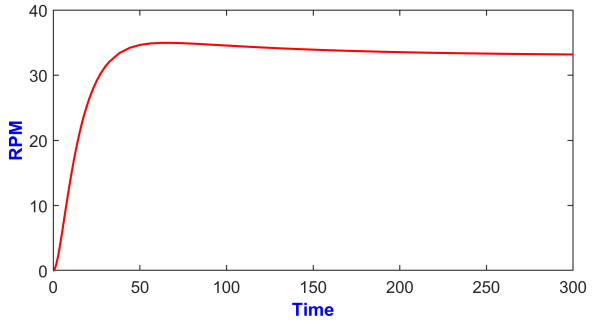

Fig. 11: Control system time response.

D. Results

To evaluate the effectiveness of the prototype and the proposed control law, tests were carried out to verify its ability to reach the RPM established above (33 RPM, 45 RPM, and 78 RPM,) and analyze both the response in terms of speed achieved and the stability and stabilization time.

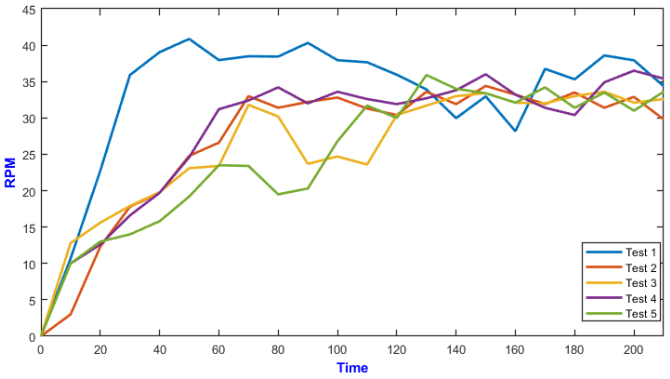

Fig. 12: Experimental speed response of the platform at 33 RPM.

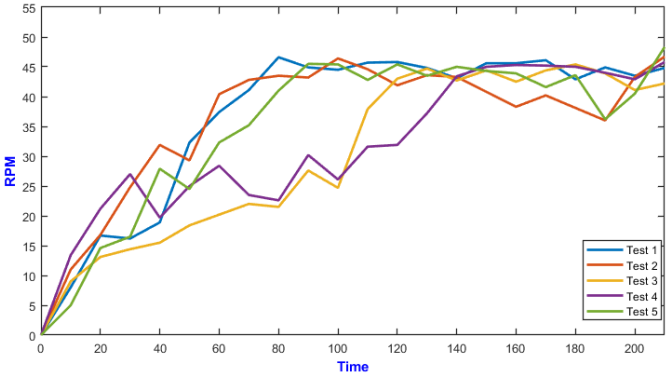

Fig. 13: Experimental speed response of the platform at 78 RPM.

1) Tests at 33 RPM: In the tests performed for 33 RPM (see Figure 12), the system reaches the target speed with minimal variation between trials. The average measured speed is close to 33 RPM, with small deviations indicating good controller performance at this operating range. The acceleration phase shows a transition of approximately 60 seconds to reach the steady state, confirming that at low speeds, the system's inertia and external disturbances have a reduced impact.

2) Tests at 45 RPM: The tests for 45 RPM (see Figure 13) exhibit a similar response, although with slightly higher variability during the acceleration phase. The average speed attained is around 45 RPM, with dispersion slightly greater than that observed at 33 RPM. While the PI controller is effective at maintaining the steady speed once reached, the transition to steady state shows variations likely due to differences in initial conditions or fluctuations in the Hall sensor signal.

3) Tests at 78 RPM: For the 78 RPM tests (see Figure 14), the data show a more complex response. All five tests indicate that although the system eventually reaches the target speed, within a range from approximately 120 seconds to 360 seconds, there is greater dispersion during both the acceleration and stabilization phases. This translates into significantly longer settling times (on the order of several minutes) and higher variability in the measured speed, suggesting that at high speeds, the system's inertia and the limitations of the magnetic actuators and sensor feedback have a more pronounced effect on overall performance. Additionally, increased

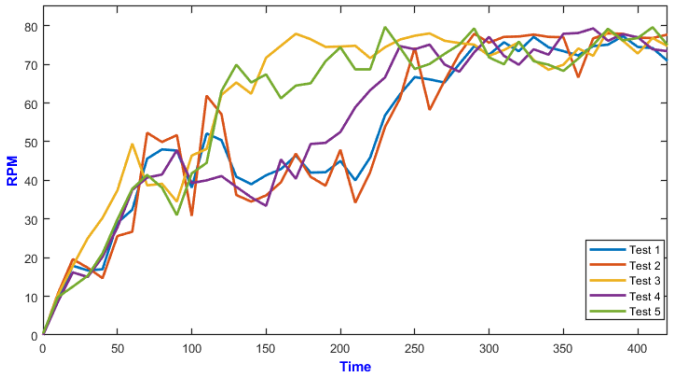

Fig. 14: Response of 5 tests at 78 RPM.

noise in the signal is observed, possibly due to the system's heightened sensitivity to environmental disturbances at these speeds.

III. Discussion

At low-speed regimes (33 and 45 RPM), the prototype exhibited a consistent response and rapid stabilization, indicating that the implemented PI controller effectively compensates for disturbances and maintains a stable speed. In contrast, at 78 RPM, an increase in response variability and longer stabilization times were observed. The greater dispersion in the data suggests that factors such as system inertia and environmental disturbances more significantly impact the controller's ability to achieve and maintain the desired speed.

When compared with previous studies [3], [4], the control strategy based on a transfer function derived from the system's inverse curve proved sufficient for implementing functional control. However, while other approaches have utilized advanced control methods or specific optimization techniques to minimize friction and enhance stability in Maglev applications, our prototype highlights the need for further adjustments in the controller for high-speed operations. In this regard, the integration of more flexible control methods or those based on artificial intelligence may yield improved performance.

Overall, the results suggest several future research directions, including further optimization of the controller to enhance performance at high speeds, exploration of adaptive control strategies, and the integration of higher-precision sensors to minimize noise in the feedback.

IV. Conclusion

In this work, we have presented the design and control of a magnetic levitation and rotation system applied to a 30 cm platform, utilizing Maglev technologies to reduce mechanical wear and friction. A prototype was developed based on a magnetic levitator capable of supporting up to 700 g and a circular array of 12 electromagnets, which, through a controlled on/off sequence, generates the angular motion of the levitated platform. The integration of permanent magnets and electromagnets enabled a system that achieves stable suspension and precise speed regulation, using an adaptive PI controller with feedback provided by a Hall effect sensor employed as a tachometer.

The experimental analysis demonstrated acceptable performance at low speeds and a more complex behavior at high speeds, due to system inertia and the inherent limitations of the electromagnets. The results confirm the feasibility of the proposed design for low-maintenance rotational applications and provide a solid foundation for future research. Future work should focus on optimizing the control for high-speed regimes, improving feedback robustness, and integrating new control strategies to further reduce variations in the system's response.

References

[1] J. Kim, C. W. Ha, G. B. King, and C. H. Kim, "Experimental development of levitation control for a high-accuracy magnetic levitation transport system," *ISA Transactions*, vol. 101, 2020.

[2] S. R. Dabbagh, M. M. Alseed, M. Saadat, M. Sitti, and S. Tasoglu, "Biomedical applications of magnetic levitation," 2022.

[3] H.-W. Cho, J.-S. Yu, S.-M. Jang, C.-H. Kim, J.-M. Lee, and H.-S. Han, "Equivalent magnetic circuit based levitation force computation of controlled permanent magnet levitation system," *IEEE Transactions on Magnetics*, vol. 48, no. 11, pp. 4038–4041, 2012.

[4] H.-W. Cho, H.-S. Han, J. Lee, B.-S. Kim, and S.-Y. Sung, "Design considerations of em-pm hybrid levitation and propulsion device for magnetically levitated vehicle," *IEEE Transactions on Magnetics*, 2009. [Online]. Available: http://doi.org/10.1109/tmag.2009.2023998

[5] B. Cullity and C. Graham, "Introduction to magnetic magnetic materials, second edition," *IEEE Pres & Wiley, New Jersey, USA*, 2009.

[6] J.-H. Jeong, C.-W. Ha, J. Lim, and J.-Y. Choi, "Analysis and control of electromagnetic coupling effect of levitation and guidance systems for semi-high-speed maglev train considering current direction," *IEEE Transactions on Magnetics*, vol. 53, no. 6, pp. 1–4, 2017.

[7] I. Boldea, L. N. Tutelea, W. Xu, and M. Pucci, "Linear electric machines, drives, and maglevs: An overview," *IEEE Transactions on Industrial Electronics*, vol. 65, 2018.

[8] F. Safaei, A. A. Suratgar, A. Afshar, and M. Mirsalim, "Characteristics optimization of the maglev train hybrid suspension system using genetic algorithm," *IEEE Transactions on Energy Conversion*, 2015. [Online]. Available: http://doi.org/10.1109/tec.2014.2388155

[9] H. Ucar, "Polarity free magnetic repulsion and magnetic bound state," *Symmetry*, vol. 13, no. 3, 2021. [Online]. Available: https://www.mdpi.com/2073-8994/13/3/442